Journal of Science and Transport Technology
Journal homepage: https://jstt.vn/index.php/en

Pre-stressed Ultra High Performance Concrete Slab Subjected to Blast Impact - A numerical study

Ba Danh Le[1], Trong Lam Nguyen[1], Viet Chinh Mai[2,*], Chi Hieu Dao[3], Tien Dat Tran[1,4]

[1]Hanoi University of Civil Engineering, Hanoi 100000, Vietnam
[2]Institute of Construction Technology, Le Quy Don Technical University, Hanoi, Vietnam
[3]Sungkyunkwan University, Sungkyunkwan-ro, Natural Sciences campus, 2066 Seobu-ro, Jangan-gu, Suwon-si, Gyeonggi-do, Korea
[4]Saitama University, 255 Shimookubo, Sakura Ward, Saitama, Japan

Article info
Type of article:
Original research paper

DOI:
https://doi.org/10.58845/jstt.utt.2025.en.5.2.84-97

***Corresponding author:**
Email address:
maivietchinh@lqdtu.edu.vn

Received: 26/03/2025
Received in Revised Form: 11/05/2025
Accepted: 27/05/2025

Abstract: The purpose of this article is to study the blast resistance capacity of Pre-stressed Ultra High Performance Concrete slab. Three-dimensional numerical models, including the explosion source, Ultra High Performance Concrete (UHPC) slab reinforced by pre-stressed tendons and steel bars under boundary conditions, are developed to simulate the full-scale behavior of the structure under blast load. The proposed simulation model is validated through comparison with the results of a prior experimental study. Chosen explosions with the stand-off distance and TNT charge weight in two cases of close-in and near-field regime. The analysis results are compared to the UHPC slab reinforced by steel bars and High Strength Concrete (HSC), with a focus on blast resistance capacity and the level of damage reduction in the structure. The results of the analysis indicate that HSC slabs sustain a 70% higher level of severe damage compared to UHPC slabs reinforced with pre-stressed tendons. The dynamic increase factor of UHPC is determined to be 32% larger than HSC. Concerning UHPC slabs, while the pre-stressed tendon serves as crucial in decreasing deflection of slabs under blast loads, its influence on altering the damage level of the structure is less pronounced.

Keywords: Pre-stressed slab; Ultra High Performance Concrete (UHPC); damage; KCC model; high strength concrete (HSC).

1. Introduction

Recently, due to economic development and the demand for a safe life, structural design to resist special loads like blast load has become more urgent. Therefore, studying the performance of structural components of construction like columns, slabs, girders, etc. against extreme loading scenarios is necessary. Reinforced concrete is a conventional material utilized for military and civilian construction to resist the effect of an explosion [1]. Numerous studies have been conducted on conventional reinforced concrete components, including columns [2-4], beams [5-7], slabs [8-10], frames [11, 12], walls [13, 14] and others [15] subjected to blast loads. Based on these studies, one sees that reinforced concrete

(RC) exhibits many advantages for structures subjected the explosion. However, large deformation and extensive damage degree in tension are known as the downsides of the RC structure [16, 17].

In the construction field, fiber reinforced concrete in general [18-20] and UHPC in particular can be considered as an advanced material [21]. Although UHPC has been under research for over a quarter of a century, compared to conventional concrete it is still a relatively new material. The rigorous requirements in the particle composition and mix design of UHPC result in superior properties both in mechanics and physics compared to normal concrete. Experimental study on UHPC slabs subjected to the explosion impact is meager because of cost and safety requirements that limit the application of UHPC in real construction. Cavili and Rebentrost [22] performed some explosive tests on seven panels made from reactive powder concrete, a type of UHPC material. The findings of these studies suggest that compared to reactive powder concrete (RPC) panels, the normal reinforced concrete panel are more severe damage, including spalling and fragmentation state. By contrast, the RPC panel resists spalling and fragmentation, that might results in a danger to humans and the infrastructure. Wu et al. took tests to investigate the behavior of UHPC slabs with and without reinforcement, slabs reinforced by polymer fibers and conventional reinforced concrete slabs under an explosion impact [23]. According to obtained results, conventional concrete slabs suffered more seriously damaged than UHPC slabs. In addition, UHPC slabs reinforced by FRP plates show a larger blast loading capacity. Barnett performed the tests of UHPC plates subjected to the blast of 100kg of TNT-equivalent explosion. They hold the view that UHPC material possesses superior properties for withstanding the impact of blast loading [24]. Ellis et al. implemented the tests of UHPC plates under blast impact to study a multi-scale model. They concluded that the geometry of fiber and volume fractions are essential to resist blast loading.

Current work investigates the behavior of Pre-stressed Ultra High Performance Concrete (PUHPC) slabs under the explosion condition. The slabs with dimension of 3000mm x 1000mm x 15mm are simulated under the close-in and near-field regime of a source of the explosion. The blast load is assumed equivalent to 8 kg of TNT. The development of simulation models is accomplished via the application of the ABAQUS software. Deflection and strain of a UHPC slab without pre-stressed tendons as well as an HSC slab are analyzed to highlight the important role of pre-stressed tendons. The damage state of the slab, a crucial parameter, is also investigated.

2. Materials and methods

2.1. Geometric modelling

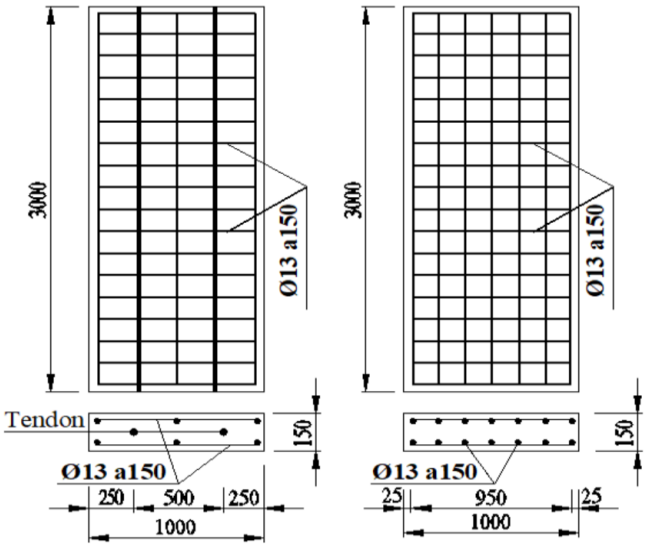

Fig. 1. Configuration of PUHPC slab (A) with pre-stressed tendon, UHPC (B) and HSC slab (C) without tendon

The numerical simulation study encompasses three scenarios: (1) a UHPC slab reinforced with pre-stressed tendons (PUHPC), (2) a UHPC slab without pre-stressed tendons and (3) a high-strength concrete slab. Slabs in scenarios 2 and 3 contains steel bar reinforcements. In the PUHPC slab, the bar reinforcement content is reduced by 50%. Pre-stressed tendons have a place in the middle of the structure to avoid the creation of a pre-camber within the slab, thereby

providing a basis for comparing the displacements induced by blast loads with scenarios two and three. Dimension and details of slabs are provided in Fig. 1 and Table 1.

Table 1. Details of slabs

Slab	Detail	Dimension (m)	Steel reinforcement bar by volume (%)
A (PUHPC)	Pre-stressed UHPC slab	3x1x0.1	1.25
B (UHPC)	UHPC slab	3x1x0.15	2.5
C (HSC)	High strength concrete slab	3x1x0.15	2.5

Pre-stressed tendons used in the PUHPC slab are the 15.2mm mono-strand, type of SWPC7A, as specified in the Korean standard [25]. D13 steel type of SD400 is used for reinforcement. Table 2 details the technical parameters of the pre-stressed tendons, which include the yield value of 1471 MPa and an ultimate strength of 1860 MPa. The tendons are pre-stressed with an axial force equivalent to 70% of the yield strength. The characteristics of the SD400 bar reinforcement indicate the yield value of 400 MPa and the ultimate strength of 560 MPa. Fig. 2 shows the stress-strain curves of tendons and steel bar reinforcement.

Table 2. Technical specifications of pre-stressed SWPC7A tendons and SD400 mild steel bars

Material	Diameter (mm)	Modulus of elasticity (GPa)	Yield strength / Ultimate strength (MPa)
SD400	13	200	400/560
SWPC7A	15.2	200	1471/1860

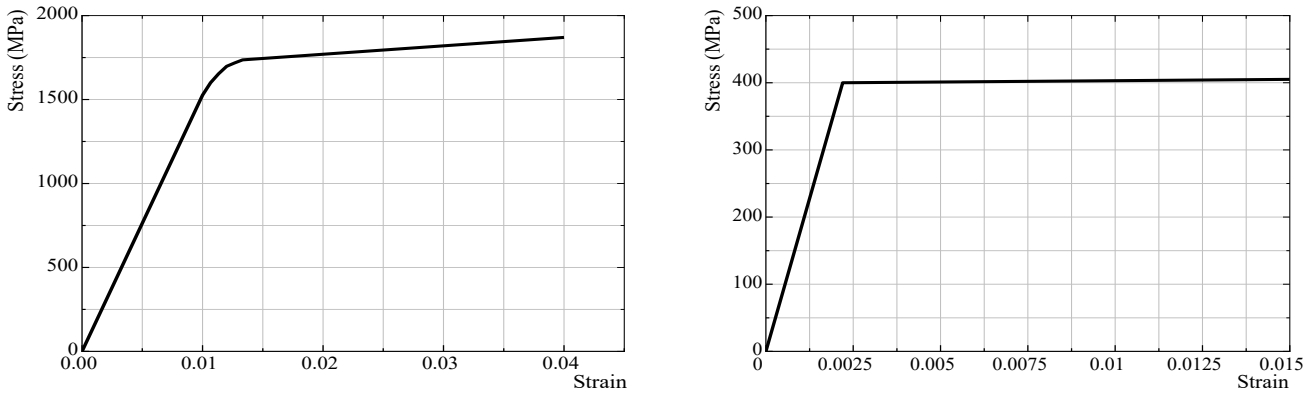

(a) SWPC7A (b) SD400

Fig. 2. Stress - strain curve of pre-stressed SWPC7A tendons (a) and SD400 steel bars (b)

2.2. Concrete material model

The Kargozian-Case (KCC) concrete material model provides an effective tool to simulate the behavior of concrete material under dynamic impact, including the projectile, blasts, and seismic events. The KCC model was initially introduced by Malvar et al. [26, 27]. Subsequent research has focused on improving the KCC model [28]. Developed to address the limitations of traditional concrete models, the KCC model incorporates advanced constitutive relationships that capture the complicated nonlinear characteristics of concrete, involving influence of strain rate or material failure. This model is particularly useful to investigate the response of concrete structures under the condition of high strain rate, providing an accurate and reliable framework for engineering analysis and design. A critical component of the KCC model is the implementation of the Dynamic Increase Factor (DIF), which accounts for the rate-dependent enhancement of material strength under dynamic loading. The DIF is introduced into the KCC model by modifying the failure surfaces to reflect the observed increase in strength with strain rate. This rate effect can be implemented either through user-

defined input in ABAQUS or internally through built-in functions. In this study, the DIF of UHPC is established in accordance with the recommendations of the CEB-FIP code [29], with a typical strain rate of 30 s^{-1} used for blast simulations. For HSC, similar strain-rate-dependent enhancements are adopted based on recognized models. The material parameters used in the simulation are referenced from two main sources. First, the quasi-static mechanical properties (e.g., compressive strength, tensile strength, Young's modulus, and fracture energy) of UHPC and HSC were obtained from published experimental data. Second, the dynamic strength enhancements were derived using empirical expressions consistent with the CEB-FIP model and verified against validated test results. Table 3 presents the input parameters for UHPC and HSC used in the KCC model [30].

Table 3. Material parameters of UHPC and HSC [30]

Variable	Description	UHPC	HSC
ρ (Ton/mm^3)	Density	2.4e^{-9}	2.4e^{-9}
f_c (MPa)	Compressive strength	126.8	80
f_t (MPa)	Tensile strength	11.03	5.95
E (MPa)	Young's modulus	43500	30300
F (kJ/m^2)	Fracture energy	17.04	11.3
P	Poisson's ratio	0.19	0.19

In the simulation model, the C3D8R element is utilized to simulate the UHPC slab. C3D8R is a three-dimensional element that contains eight nodes, three degrees of freedom and is capable of being translated in the directions of x, y, and z. The pre-stressed tendon and reinforcements are simulated by the T3D2T element. It can be assumed that only deformation due to axial stress occurs in the T3D2T element [31]. The finite element mesh model of PUHPC, UHPC and HSC slab are shown in Fig. 3. The mesh convergence study is conducted using several mesh sizes ranging from 10 mm to 30 mm within the slab domain. The results indicate that refining the mesh from 30 mm to 15 mm significantly enhances the accuracy, particularly in capturing deflection and local damage. However, further refinement below 15 mm yields only marginal improvements in simulation accuracy while substantially increasing computational costs. Consequently, a mesh size of 15 mm is selected as the optimal compromise between computational efficiency and result reliability.

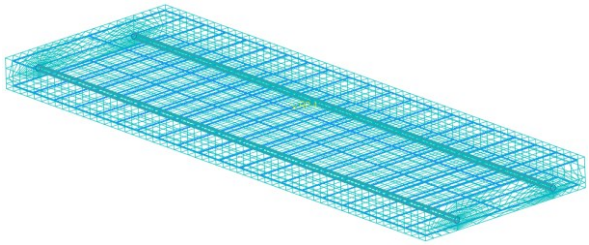

(a) Slab A with presstressed tendons

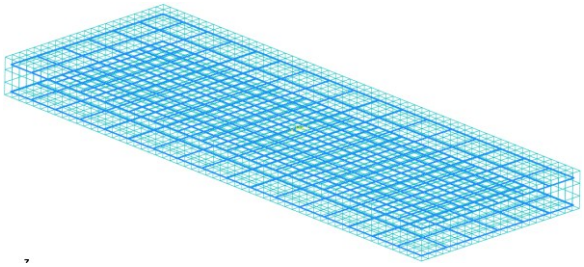

(b) Slab B, C without tendons

Fig. 3. Mesh model of PUHPC slab (A) and UHPC, HSC slab (B, C)

2.3. Blast loading and boundary condition

The Coupled Eulerian-Lagrangian (CEL) technique is a sophisticated numerical approach utilized in blast loading simulations to accurately capture the complex interactions between explosive materials and structural components. Unlike traditional methods, CEL enables the simultaneous modeling of fluid and solid mechanics by combining Eulerian elements, which are suitable for representing fluid-like explosive materials. This hybrid technique allows for a more realistic and detailed simulation of the blast wave propagation and the impact on structural components, accommodating large deformations and material failure. Consequently, CEL is particularly valuable in assessing the blast resistance of advanced materials such as UHPC. The ideal gas equation is incorporated in the CEL simulation to model air movement, utilizing parameters density, EOS, specific heat, and

viscosity. These parameters are available in the referenced document [32]. Table 4 provides the parameters of TNT explosives used in the CEL simulation.

Table 4. Parameters of TNT for the CEL simulation model

Type	Property	Value	Unit
Density	Mass Density	1630	kg/m^3
JWL EOS	Detonation wave speed	6930	m/s
	A	37377e^{07}	N/m^2
	B	37471e^{05}	N/m^2
	ω	0.35	//
	R1	4.15	//
	R2	0.9	//

The equation below defines the relationship between the charge weight of the explosive (W) and the stand-off distance from the blast loading (R) [33, 34]:

$$Z = \frac{R}{W^{1/3}} \quad (1)$$

The blast loading condition in each regime are quantified by calculating the scaled distance (Z) [35], as shown in Table 5.

Table 5. Response regime according to the Smith et al. (2009) [35]

Scaled distance	Z (m/kg1/3)
Close in	Z ≤ 1.19
Near field	1.19 < Z ≤ 3.97

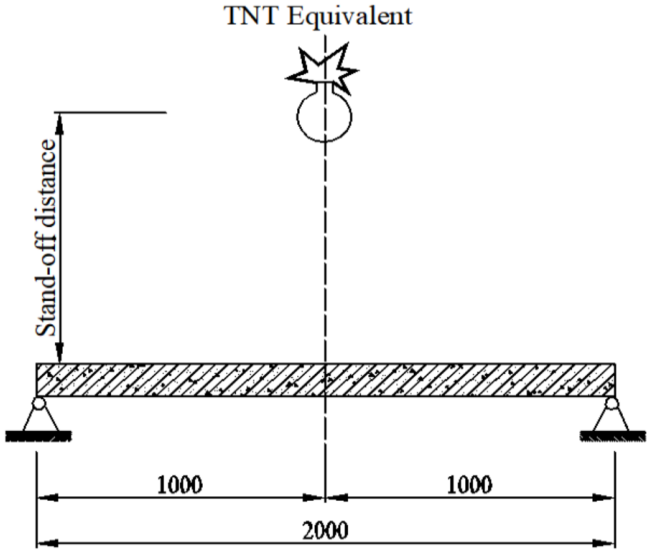

Fig. 4. Boundary condition of the simulation model

The boundary conditions are defined as simply supported at both ends of the slab, as illustrated in Fig. 4. In the numerical simulation, this is implemented by fully constraining the vertical (Z-direction) and transverse (X-direction) displacements at both slab ends, thereby effectively restraining slab rebound and minimizing lateral movement. These boundary constraints are applied to ensure accurate simulation of the structural response under blast loading.

3. Results and discussion

3.1. Simulation validation

The simulation model employed in the present study is validated by comparison with the test results of Wu et al. [23]. Wu conducted tests on the blast loading behavior of a UHPC slab without reinforcements. The detailed dimensions of the slab is shown in Fig. 5. UHPC used in the study possess a compressive strength of 151.6 MPa, a tensile strength of 30.2 MPa, and an elastic modulus of 47000 MPa. The UHPC slab is tested to an explosive charge equivalent to 3.4 kg of TNT, positioned at a distance of 0.75 m from slab's surface. According to Eq. 1, the scaled distance (Z) is calculated to be 0.5 (m/kg$^{1/3}$). The data acquisition device sustains damage when subjected to explosion testing with pressures exceeding 6 MPa. Fig. 6 and Table 6 show the pressure history at the point near the specimen support determined by both experimental testing and simulation. The differences observed in the pressure history curve between the test and simulation are primarily attributed to both experimental uncertainties and limitations inherent in numerical modeling. In the experimental setup, factors such as variations in detonation point, environmental disturbances, sensor accuracy, and wave reflections from the testing boundary may cause fluctuations in the pressure history signal. These aspects can lead to deviations in the peak value, arrival time, and oscillation pattern of the pressure curve recorded during the test. In the numerical model, the blast loading is simulated using the Coupled Eulerian-Lagrangian (CEL) technique, which provides a more detailed representation of blast wave propagation and its

interaction with the surrounding air and structural surfaces. However, even with the CEL approach, idealizations in initial conditions may still contribute to differences when compared to real-world tests. Despite these differences, the simulation results capture the general trend and magnitude of the pressure-time history with sufficient accuracy. The peak reflected pressure and the impulse value are reasonably close to the experimental measurements.

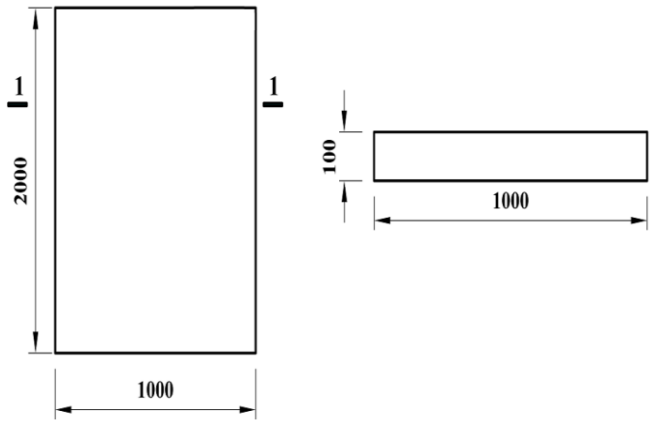

Fig. 5. Geometry of specimens in the test of Wu [23]

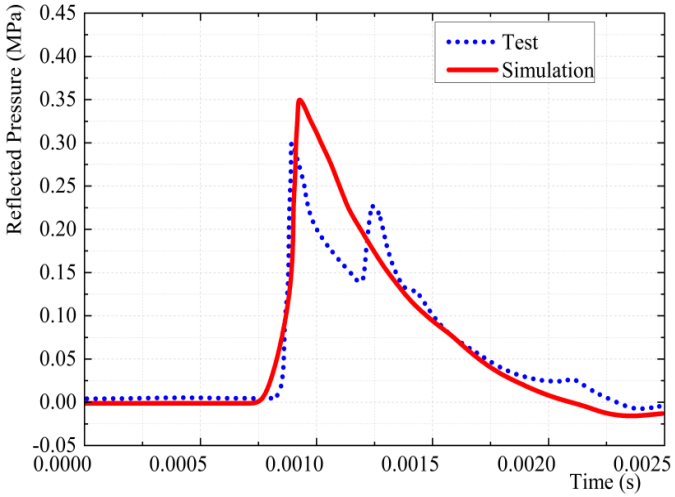

Fig. 6. Pressure history on the blast test of Wu [23] and simulation

Table 6. Comparison of simulation and test result by Wu [23]

Case study	Peak reflected overpressure (MPa)	Disp. (%)	Maximum deflection (mm)	Disp. (%)
Wu's test	0.3	//	13.2	//
Sim.	0.35	16.7	15.1	14.3

Fig. 7 confirms that the blast wave uniformly covers the entire slab surface in the simulation, reproducing the experimental boundary conditions. Fig. 8 compares the crack distribution at the bottom surface of the slab, revealing that cracks in the simulation are slightly fewer and more localized compared to those observed in Wu's test. This variation primarily stems from the assumptions in the simulation, such as the use of the material model in ABAQUS, which does not fully capture the post-cracking fiber-bridging effects and micro-crack development typical of UHPC. Additionally, the numerical model assumes ideal boundary conditions and material homogeneity, while experimental results are affected by construction imperfections and measurement uncertainties. Although these limitations exist, the crack pattern in the simulation closely follows the dominant damage mechanism observed experimentally - centralized cracking with depth extending beyond half the slab thickness. The overall agreement in failure mode, deformation characteristics, and quantitative results indicates that the proposed simulation model is sufficiently accurate for use in subsequent parametric analyses. Therefore, while slight differences exist, they are minor and do not compromise the reliability or predictive capability of the model.

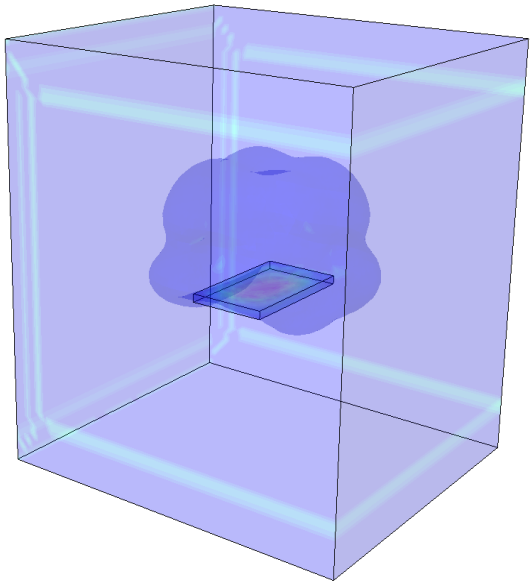

Fig. 7. Numerical simulation of the UHPC slab under blast wave

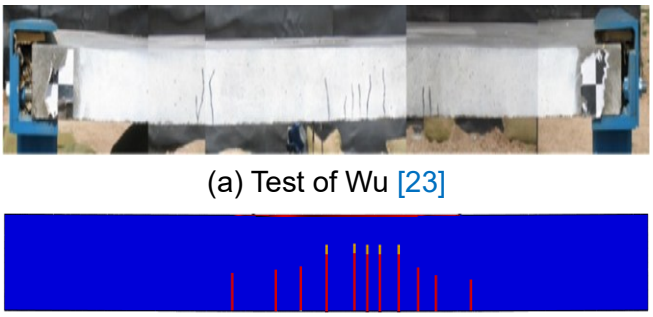

(a) Test of Wu [23]

(b) Simulation

Fig. 8. Cracks in UHPC slabs according to experimental (a) and simulated (b) results

3.2. Deflection Analysis

In this section, a detailed parametric investigation is conducted to evaluate the structural response of UHPC pre-stressed slabs under blast loading. Two representative blast scenarios are considered, classified by scaled distance into close-in and near-field regimes. As shown in Table 7, both cases use an 8 kg TNT charge, with varying standoff distances to represent different blast intensities. This setup allows for a clearer understanding of how blast proximity affects the performance and failure behavior of UHPC slabs.

Table 7. Case study in this study

Case	TNT charge weight (kg)	R (m)	Z (m/kg$^{1/3}$)	Scaled distance
1	8	2	1.0	Close-in
2	8	4	2.0	Near field

Table 8 and Fig. 9 show the maximal deflection at the mid-span of slabs. In the 4m stand-off distance, it can be seen that no large difference in the deflection of all slabs. The maximal deflection corresponding to the PUHPC slab, UHPC slab, and HSC slab, is 9.2 mm, 10.2 mm, and 11.4 mm, respectively. However, in regards to a stand-off distance of 2 m, the maximal deflection at the mid-span increases remarkably. The maximal deflection represents 13.18 mm, 21.2 mm, and 29.1 mm in PUHPC, UHPC, and HSC slabs, respectively. The stand-off distance affects considerably the deflection of the slab. On the other hand, in both close-in and near field regimes, the maximal deflection at the mid-span of the HSC slab is larger than the UHPC slab. For example, at a scaled distance of 1 in the first scenario, the maximal deflection of the HSC slab is 220% and 137% greater than that of the UHPC and PUHPC slabs, respectively. This demonstrates that, in comparison to HSC material, UHPC material significantly reduces the displacement of the slab under blast loading.

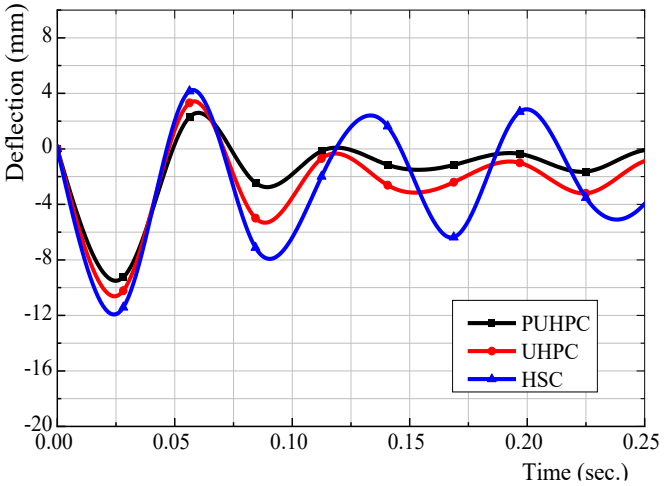

(a) 4m stand-off distance

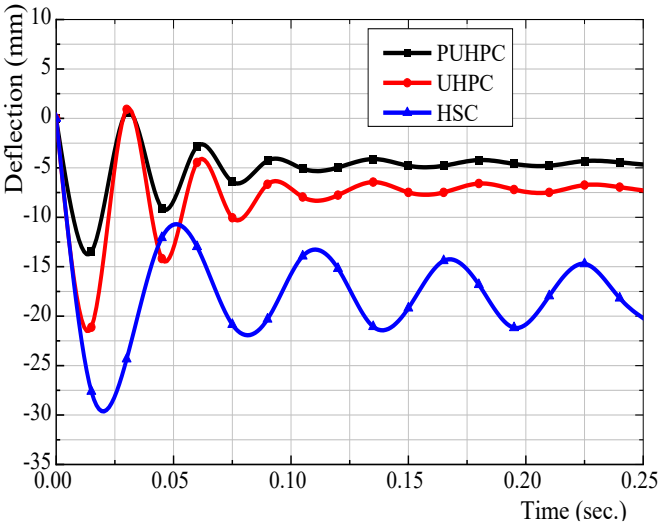

(b) 2m stand-off distance

Fig. 9. Maximum deflection at the middle span of slab in 4m (a) and 2m stand-off distance (b)

Let us now examine the impact of pre-stressed tendons on the maximal deflection of the UHPC slab. The deflection increments for the three slabs, PUHPC, UHPC, and HSC under scenarios 1 and 2 are 150% (13.18/9.2), 207% (21.2/10.2), and 255% (29.1/11.4), respectively. The findings unequivocally demonstrate the significant effect of pre-stressed tendons in minimising the deflection

of the slab under blast pressures. Additionally, the maximal deflection at the mid-span of the PUHPC slab tends to approach zero more rapidly compared to the UHPC slab. In other words, after the blast loading impact, the PUHPC slab stabilizes more quickly than the UHPC and HSC slabs.

Table 8. Maximum deflection at the middle span of slabs

Slab	Deflection (mm) Stand-off distance 2m	Deflection (mm) Stand-off distance 4m
PUHPC	13.18	9.2
UHPC	21.2	10.2
HSC	29.1	11.4

3.3. Strain Results

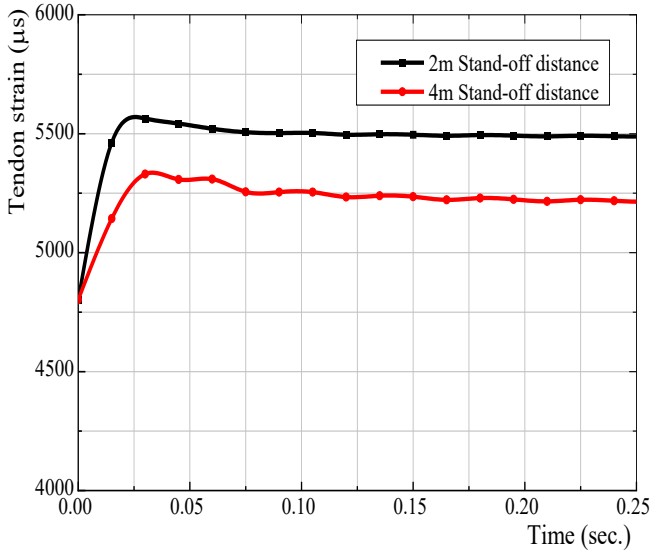

Fig. 10. Strain of pre-stressed tendon (4m stand-off distance and 2m stand-off distance)

Fig. 10 shows the time-history response of tensile strain in the pre-stressed tendon under two different stand-off distances of 2 m and 4 m. Prior to blast loading, the tendons are pre-tensioned to 70% of their yield strength to simulate the actual prestressing condition in typical structures. Upon the arrival of the blast wave, there is a sharp increase in tensile strain due to the sudden dynamic effect. In Scenario 1 (2 m stand-off distance), the tendon strain reaches a peak of 5563.79 με, while in Scenario 2 (4 m stand-off), it reaches 5330.51 με. The higher strain in the 2 m case reflects the greater intensity of blast pressure transmitted to the structural elements at closer proximity. Fig. 10 also clearly shows the stabilization trend of strain over time after the peak, indicating the dissipation of blast energy and the return toward equilibrium. Throughout the blast event, the tendons remain in tension, confirming that the prestressing effect is preserved under impulsive loading. This time-dependent strain behavior complements the overpressure distribution shown in Fig. 7, offering insight into how external blast loads translate into internal stress responses of key structural components.

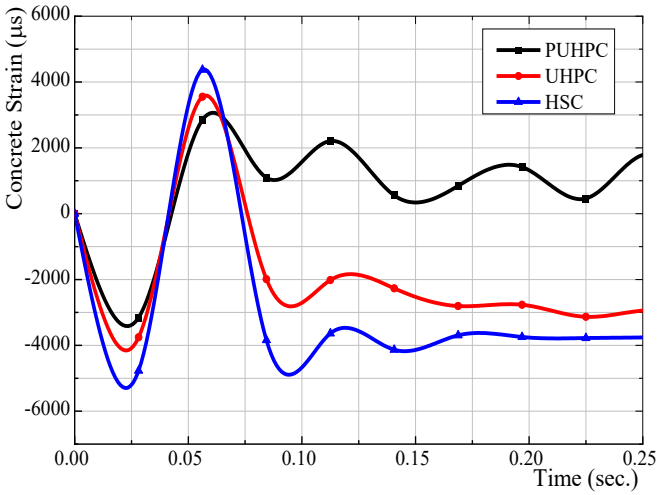

(a) 4m stand-off distance

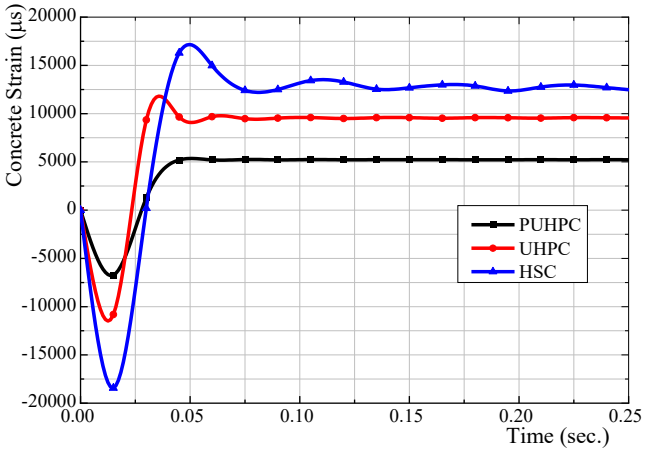

(b) 2m stand-off distance

Fig. 11. Strain of concrete elements in 4m (a) and 2m stand-off distance (b)

Figs. 11 and 12 show the strain value of the concrete element and steel bars. Acquired outcomes show a substantial rise when the stand-off distance declines from 4 m to 2 m. For instance, the maximal compressive strain observed in PUHPC, UHPC, and HSC slabs at the stand-off

distances of 4 m is -3154.5 μs, -3755.6 μs, and -4770.6 μs, respectively. These values increase by factors of 2.1, 2.9, and 3.8, corresponding to -6732.7 μs, -10816.1 μs, and -18433.8 μs, respectively. Results indicate that PUHPC slabs exhibit the smallest strain compared to UHPC, and HSC slabs. The compressive strain in the steel reinforcing bars of HSC slab is the highest, whereas the PUHPC slab exhibits the lowest strain. For instance, at the stand-off distance of 2 m, the strain in steel bars of HSC slab is 1.7 and 2.3 times greater compared to PUHPC and UHPC slab, respectively. The strain difference between PUHPC and UHPC slab is relatively smaller, with ratios of 1.3 and 1.4 times, respectively, for stand-off distances of 2 m and 4 m.

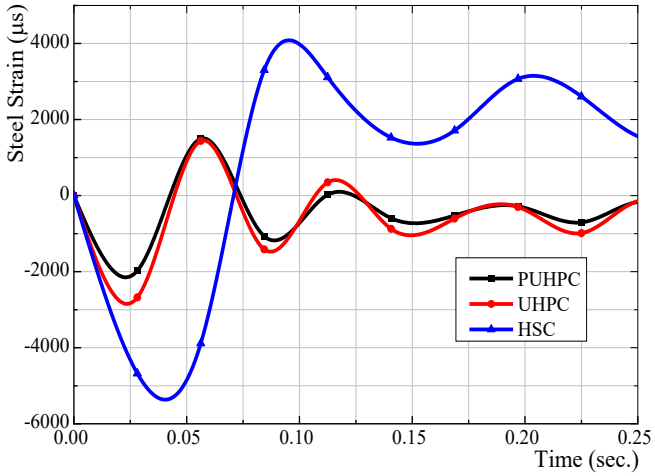

(a) 4m stand-off distance

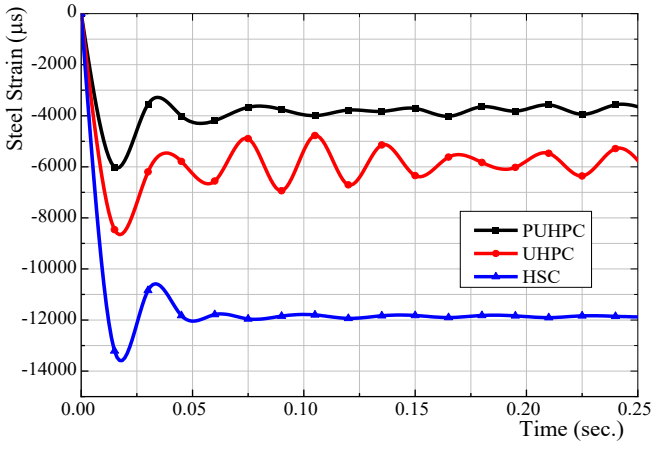

(b) 2m stand-off distance

Fig. 12. Strain of steel bars in 4m (a) and 2m stand-off distance (b)

UHPC is a relatively new material and there remains considerable controversy regarding its dynamic behavior [36]. According to guidelines of the CEB-FIP Code [29], the DIF of concrete can be determined by equation:

$$DIF = \frac{f_c}{f_{cs}} = \begin{cases} (\dot{\varepsilon}/\dot{\varepsilon}_s)^{1.026\alpha} \text{ for } \dot{\varepsilon} \le 30\,s^{-1} \\ \gamma_s(\dot{\varepsilon}/\dot{\varepsilon}_s)^{1/3} \text{ for } \dot{\varepsilon} > 30\,s^{-1} \end{cases} \quad (2)$$

f_c refers to the dynamic compressive strength of the material at the strain rate $\dot{\varepsilon}$; f_{cs} denotes the static compressive strength at strain rate $\dot{\varepsilon}_s$; ε is regarded as the range of the strain rate between $30s^{-1}$ to $300s^{-1}$;

$\gamma_s = 6.156\times\alpha - 2$; $\alpha = (1/5+9\times f_{cs} / f_{c0})$;

$f_{c0} = 10MPa$.

Table 9 summarizes the dynamic strength in compression and DIF of UHPC, HSC material. The dynamic stress and strain rate values are derived from simulations. The dynamic stress increment results in arise in strain rate. Dynamic stress corresponds to the compressive strength in this study are 1.48 and 1.96 times larger compared to static state for HSC and UHPC, respectively. The DIF of UHPC is 32% greater in comparison to that of HSC. This may be attribute to the enhanced microstructure of UHPC, that includes denser particle packing, reduced porosity, and fiber addition, resulting in superior performance under dynamic loading. A higher DIF indicates better strength retention and increased resistance to extreme condition of an explosion. The trend of DIF relates to the more serious level of failure and spalling of the HSC slab, that is discussed in the following section.

Table 9. Dynamic increase factor (DIF)

Material	Static compressive strength (MPa)	Dynamic stress (MPa)	Strain rate (s^{-1})	Dynamic increase factor (DIF)
UHPC	126.8	248.2	86.9	1.96
HSC	80	118.5	86.9	1.48

3.4. Damage Results

The damaged state of slabs in two scenarios of the explosion is shown in Figs. 13, 14, 15, 16 and Tables 10, 11. In general, the simulation results

show that under close-in and near-field blast loading, the initial damage occurs at the top surface of the slab, directly beneath the detonation point. This includes localized crushing and spalling caused by the immediate transmission of high-intensity compressive shock waves. As the blast wave propagates through the slab thickness, tensile effects develop on the rear surface, leading to the formation of flexural cracks. These cracks initiate at the underside of the slab and propagate upward, driven by the bending moment induced by the reflected overpressure. The damage is most concentrated near the center of the slab, where the dynamic stresses reach their peak. This sequence of failure mechanisms, front face crushing followed by rear face cracking, is consistent with the expected response of reinforced concrete slabs subjected to blast loading.

D is the damage variable that spans from 0 to 1. Light damage corresponds to D values between 0 and 0.2, moderate damage ranges from 0.2 to 0.6, and severe damage occurs when D exceeds 0.6. Additionally, the most severe level of damage is the complete collapse of the slab. As decreasing the stand-off distance from the blast, the damage level of slabs for all materials increases, concentrating in the mid-span as well as near the support of slabs. However, the HSC slab is more serious damage than PUHPC and UHPC slabs. For example, in the case of the 2m stand-off distance, the HSC slab suffers a 22.6% severe damage percentage by volume, which is 45.8% and 70% larger than 13.3% and 15.5% of the PUHPC and UHPC slab.

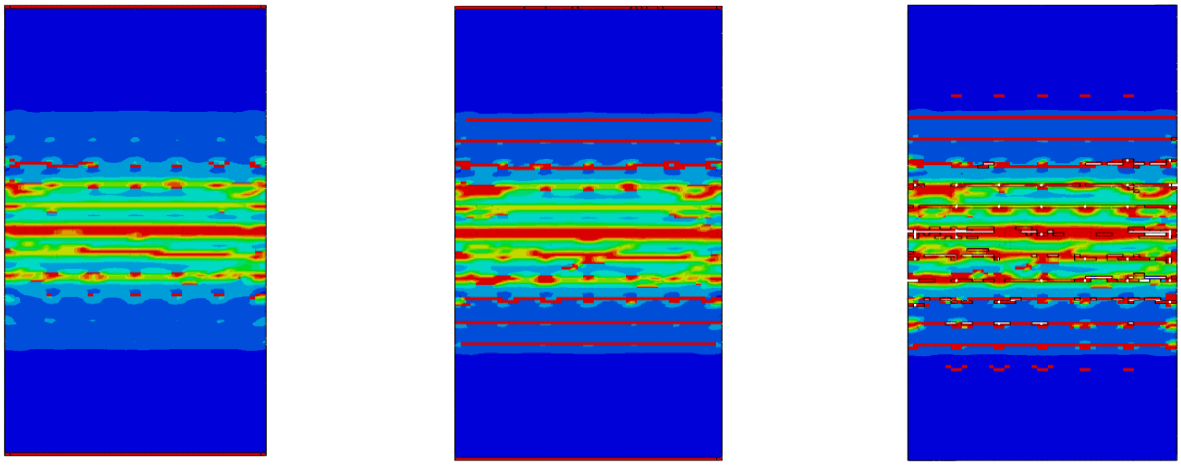

(a) PUHPC (b) UHPC (c) HSC

Fig. 13. Damage level of front face in slabs after blast load for 2m stand-off distance

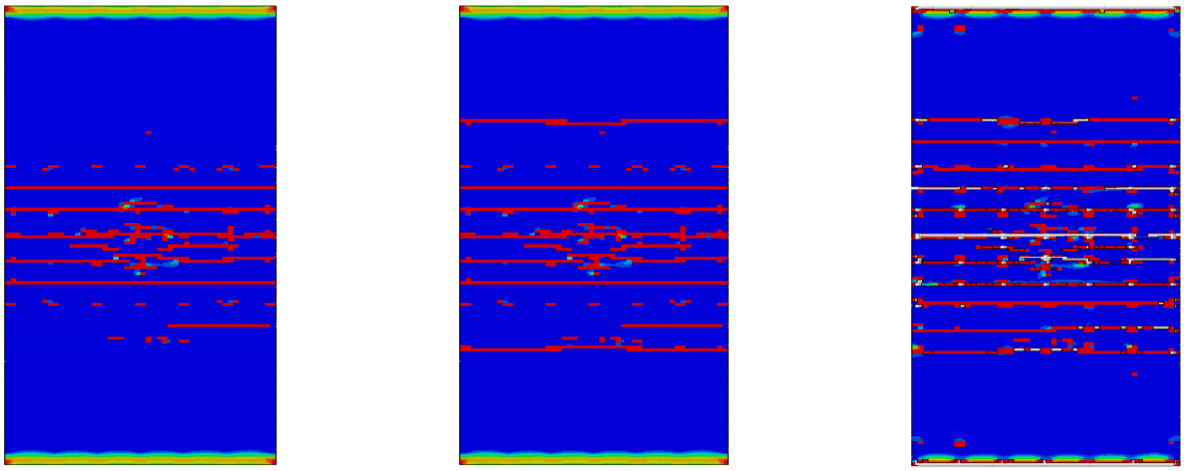

(a) PUHPC (b) UHPC (c) HSC

Fig. 14. Damage level of rear face in slabs for 2m stand-off distance

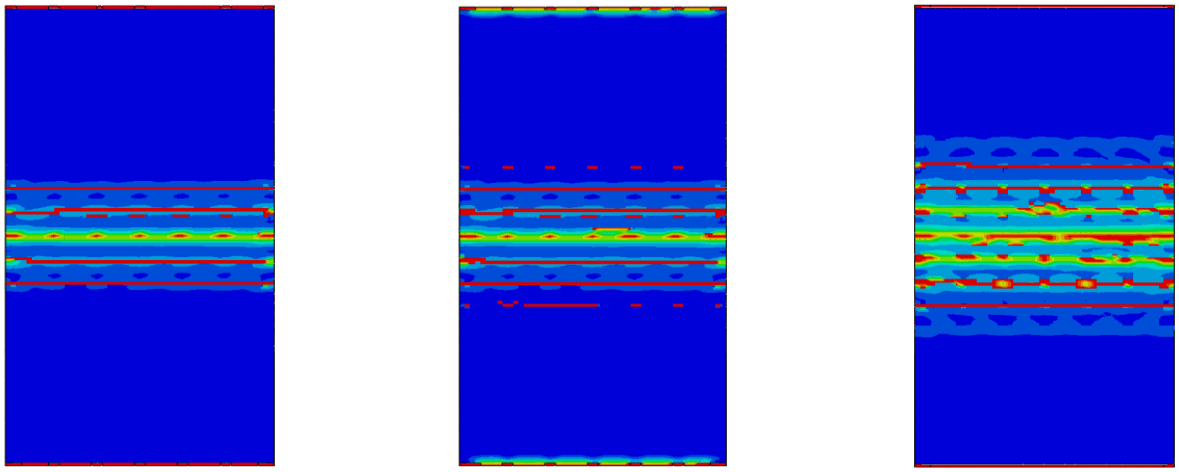

(a) PUHPC (b) UHPC (c) HSC

Fig. 15. Damage level of front face in slabs for 4m stand-off distance

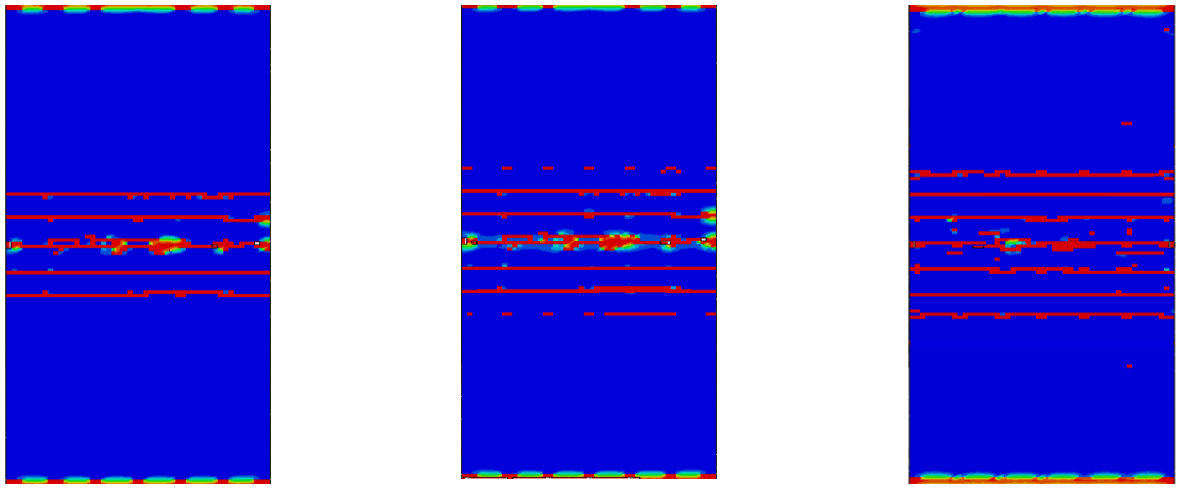

(a) PUHPC (b) UHPC (c) HSC

Fig. 16. Damage level of rear face in slabs for 4m stand-off distance

Table 10. Damage of slabs after the explosion (percentage by volume) in 2 m stand-off distance

Slab	Light damage	Moderate damage	Severe damage	Spalling
PUHPC	15.8%	17.5%	13.3%	-
UHPC	18.7%	20.2%	15.5%	-
HSC	26.1%	30.4%	22.6%	3.3%

Table 11. Damage of slabs after the explosion (percentage by volume) in 4 m stand-off distance

Slab	Light damage	Moderate damage	Severe damage	Spalling
PUHPC	7.2%	8.62%	6.9%	-
UHPC	8.42%	9.82%	8.0%	-
HSC	15.22%	14.82%	13.52%	-

A comparison of the damage state of PUHPC and UHPC slabs is performed to investigate the effect of pre-stressed tendons on the structural response under blast impact. Taking severe damage parameters for comparison as it is critical in keeping the sustainable state of structure and protecting other structures under explosion impact. In the 4m stand-off distance, the UHPC slab exhibits 8.0% severe damage by volume which is 16% higher value compared to 6.9% of the PUHPC slab. In the same way, for the 2m stand-off distance, the UHPC slab suffer 15.5% severe damage, which is 16.5% higher than 13.3% in the PUHPC slab. Although the UHPC slab shows a considerably larger deflection at mid-span in comparison with the PUHPC slab subjected to blast loading, the damage state is slightly larger than the UHPC slab. It is evident that pre-stressed tendons have a beneficial effect on reducing slab deflection under blast impact, rather than

significantly influencing the extent of structural damage.

The spall damage of the HSC slab is presented in Tables 10, 11 and Fig. 17, illustrating the typical failure mode observed in concrete structures subjected to blast loading. Spall damage occurs when the tensile stress generated by the shock wave exceeds the material's strength, causing the detachment of fragments from the back surface of the slab. These high-velocity fragments possess significant kinetic energy, posing a serious risk to human safety and potentially damaging nearby equipment. In this study, the analysis revealed that only the HSC slab exhibited spall damage, with a volume percentage of 3.3% at a stand-off distance of 2 meters. In contrast, the PUHPC and UHPC slabs remained intact without any signs of spall failure under the same loading conditions. This significant difference highlights the superior blast resistance of UHPC compared to conventional HSC material. The enhanced performance of UHPC can be attributed to its optimized microstructure, higher tensile strength, and improved energy absorption capacity, primarily due to the presence of fiber reinforcement. These findings strongly suggest that UHPC is a highly promising material for structural applications exposed to extreme blast loads, offering enhanced durability and protection against explosive threats.

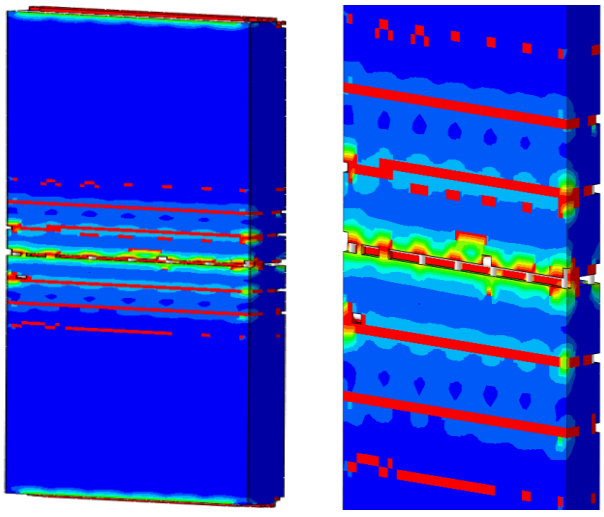

(a) Front face (b) Rear face

Fig. 17. Spall damage of HSC slab

Additional numerical simulations are conducted to assess the collapse state of HSC and UHPC slabs under blast loading. Fig. 18a shows the complete collapse of the HSC slab subjected to a 20 kg TNT equivalent explosion. Under the same conditions, although the UHPC slab sustains extensive damage still does not completely collapse, as depicted in Fig. 18b.

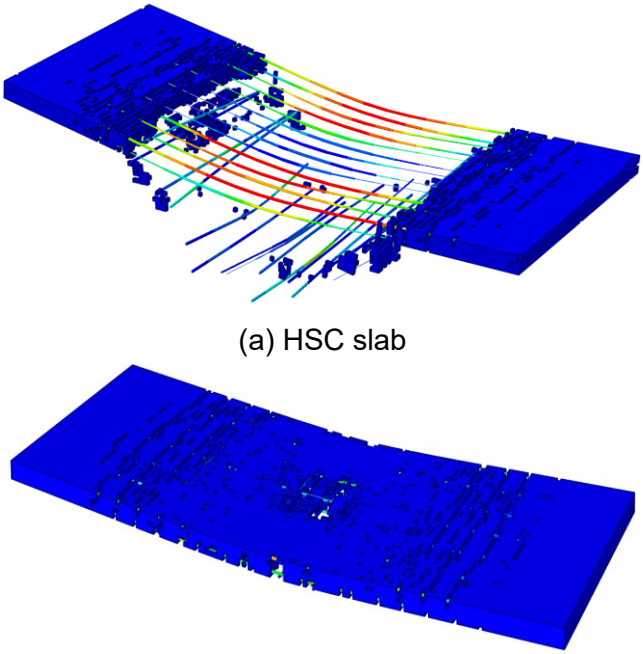

(a) HSC slab

(b) UHPC slab

Fig. 18. Collapsed state of the HSC slab (a) and severe damage of the UHPC slab (b)

4. Conclusions

This research presented the dynamic behavior results of Pre-stressed UHPC slabs under the explosion impact. Using KCC model, the simulation results are compared to the UHPC slab and HSC slab reinforced by steel bars. The following conclusions can be drawn:

1. Compared to HSC, UHPC exhibits a significantly greater capacity to resist blast loading by reducing maximal mid-span deflection, element strain, and overall damage. Under a close-in detonation regime, the HSC slab exhibits severe damage level that are 45.8% and 70% higher than those of the PUHPC and UHPC slabs. Besides, the DIF of UHPC is 32% greater than that of HSC.

2. The PUHPC slab demonstrates a smaller mid-span deflection in comparison to the UHPC

slab, while the difference in the level of damage is inconsequential. The UHPC material plays a more critical role than the pre-stressed tendons in maintaining structural integrity under explosive loads. However, pre-stressed tendons contribute to the slabs reaching the stable state more rapidly following the impact of the explosion.

Acknowledgments

This research is funded by the Ministry of Education and Training of Vietnam under grand number B2023 XDA-05.

References

[1] D. Spelman, Y.-S. Lee. (2022). Sustainability of concrete as a civil engineering material. *Engineering Journal*, 26(7), 69-81.

[2] S.-C. Lin, Z.-Q. Hu, J.-Q. Han, B. Yang, M. Elchalakani. (2023). Failure time of reinforced concrete column under blast load. *Structures*, 53, 1122-1134.

[3] Y. Liu, H. Hao, Y. Hao. (2023). Prediction of blast response of RC columns considering dynamic bond-slip between reinforcement and concrete. *Engineering Structures*, 283, 115921.

[4] Y. Shi, Y. Hu, L. Chen, Z.-X. Li, H. Xiang. (2022). Experimental investigation into the close-in blast performance of RC columns with axial loading. *Engineering Structures*, 268, 114688.

[5] M. Nagata, M. Beppu, H. Ichino, R. Matsuzawa. (2018). A fundamental investigation of reinforced concrete beams subjected to close-in explosion. *International Journal of Protective Structures*, 9(2), 174-198.

[6] W. Wei, Y.-l. Zhang, J.-j. Su, Y. Liu, F.-l. Huang. (2023). Modification of SDOF model for reinforced concrete beams under close-in explosion. *Defence Technology*, 20, 162-186.

[7] C. Yang, Z. Huang, X. Jia, W. Shang, T. Chen. (2024). Analytical model for predicting localized damage in RC beams under contact explosion. *International Journal of Impact Engineering*, 185, 104870.

[8] S.M. Anas, M. Shariq, M. Alam, M. Umair. (2022). Evaluation of critical damage location of contact blast on conventionally reinforced one-way square concrete slab applying CEL-FEM blast modeling technique. *International Journal of Protective Structures*, 13(4), 672-715,

[9] V. Kumar, K. Kartik, M.A. Iqbal. (2020). Experimental and numerical investigation of reinforced concrete slabs under blast loading. *Engineering Structures*, 206, 110125.

[10] S.-H. Sung, H. Ji, J. Chong. (2021). Experimental–theoretical investigation for damage assessment of a reinforced concrete slab under consecutive explosions based on single-degree-of-freedom model. *International Journal of Protective Structures*, 12(1), 95-109.

[11] Y.E. Ibrahim, M.A. Ismail, M. Nabil. (2017). Response of reinforced concrete frame structures under blast loading. *Procedia Engineering*, 171, 890-898.

[12] S. Zhang, C. Zhou. (2023). Study on dynamic response and safety control of reinforced concrete rigid frame structure under foundation pit blasting. *International Journal of Protective Structures*, 14(4), 549-570.

[13] J. Wu, Z. Liu, J. Yu, S. Xu. (2022). Experimental and numerical investigation of normal reinforced concrete panel strengthened with polyurea under near-field explosion. *Journal of Building Engineering*, 46, 103763.

[14] P. Panedpojaman. (2012). Modified Quasi-Static, Elastic-Plastic Analysis for Blast Walls with Partially Fixed Support. *Engineering Journal*, 16(5), 45-56.

[15] S. Dauji. (2018). New approach for identification of suitable vibration attenuation relationship for underground blasts. *Engineering Journal*, 22(4), 147-159.

[16] M. Abedini et al. (2020). Large deflection behavior effect in reinforced concrete columns exposed to extreme dynamic loads. *Frontiers of Structural and Civil Engineering*, 14, 532-553.

[17] W. Wang, Q. Huo, J.-c. Yang, J.-h. Wang, X. Wang, W.-l. Gao. (2022). Damage analysis of POZD coated square reinforced concrete slab under contact blast. *Defence Technology*, 18(9), 1715-1726.

[18] I. Prakash, T.-N. Phan, H.-V.T. Mai. (2023). Estimating the compressive strength of self-compacting concrete with fiber using an extreme gradient boosting model. *Journal of Science and Transport Technology*, 3(1), 12-25.

[19] I. Prakash, T.A. Nguyen. (2023). Predicting the maximum load capacity of circular RC columns confined with fibre-reinforced polymer (FRP) using machine learning model. *Journal of Science and Transport Technology*, 3(4), 25-42.

[20] B.-N. Phung, T.-H. Le, M.-K. Nguyen, T.-A. Nguyen, H.-B. Ly. (2023). Practical numerical tool for marshall stability prediction based on machine learning: an application for asphalt concrete containing basalt fiber. *Journal of Science and Transport Technology*, 3(3), 26-43.

[21] D.B. Le, P.T. Nguyen, H.D. Pham, V.-C. Mai, L.D. Ngo, H.X. Doan, H.T.N. Nguyen. (2025). Blast-resistant performance of UHPFRC: An experimental study and optimal steel fiber content. *International Journal of Protective Structures*, 20414196251336761.

[22] B. Cavili, M. Rebentrost. (2006). Ductal-a high-performance material for resistance to blasts and impacts. *Australian Journal of Structural Engineering*, 7(1), 37-45.

[23] C. Wu, D. Oehlers, M. Rebentrost, J. Leach, A. Whittaker. (2009). Blast testing of ultra-high performance fibre and FRP-retrofitted concrete slabs. *Engineering Structures*, 31(9), 2060-2069.

[24] S.J. Barnett, S.G. Millard, G.K. Schleyer, A. Tyas. (2010). Briefing: Blast tests of fibre-reinforced concrete panels. *Proceedings of the Institution of Civil Engineers-Construction Materials*, 163(3), 127-129.

[25] K.C. Institute. (2016). Standard Specifications for Concrete Structures.

[26] L.J. Malvar, J.E. Crawford, J.W. Wesevich, D. Simons. (1997). A plasticity concrete material model for DYNA3D. *International Journal of Impact Engineering*, 19(9-10), 847-873.

[27] L.J. Malvar, J.E. Crawford. (1998). Dynamic increase factors for concrete. DTIC document, *Defense Technical Information Center*.

[28] A. Mardalizad, M. Caruso, A. Manes, M. Giglio, G. Engineering. (2019). Investigation of mechanical behaviour of a quasi-brittle material using Karagozian and Case concrete (KCC) model. *Journal of Rock Mechanics*, 11(6), 1119-1137.

[29] C.E.-I.d. Béton. (1993). CEB-FIP model code 1990: Design code. *Thomas Telford Publishing*.

[30] O.Q. Aziz, G.H. Ahmed. (2012). Mechanical properties of ultra high performance concrete (UHPC). *American Concrete Institute, ACI Special Publication*, (289 SP), pp. 331-346.

[31] D. Systèmes. (2016). Abaqus/CAE User's Guide.

[32] B. Dobratz. (1974). Properties of chemical explosives and explosive simulants. *Lawrence Livermore Laboratory, University of California*.

[33] T. Krauthammer. (1999). Blast effects and related threats. *Penn State University.*

[34] M. Sadovskiy, P.o. Explosion. (2004). Mechanical effects of air shockwaves from explosions according to experiments. *Physics of explosion, USSR Academy of Sciences*.

[35] S.J. Smith, D.M. McCann, M.E. Kamara. (2009). Blast resistant design guide for reinforced concrete structures. Engineering Bulletin EB090.

[36] F. Huang, T. Wang, Y. Lin. (2023). Evaluation of Fastener Flexibility in Hybrid CFRP and Metal Joints Using the Finite Element Method. *Journal of Physics: Conference Series*, 2023, 02553(1), IOP Publishing, p. 012010.